Available online at www.sciencedirect.com

SciVerse ScienceDirect

Ceramics International 38 (2012) 2569–2574

CERAMICS INTERNATIONAL

www.elsevier.com/locate/ceramint

Short communication

Synthesis and photoluminescence properties of $Ba_{1-y}Sr_yLa_{4-x}Dy_x(WO_4)_7$ ($x = 0.04–0.2$, $y = 0–0.4$) phosphors

Shao-An Yan [a], Jian-Wen Wang [b], Yee-Shin Chang [c], Weng-Sing Hwang [a,*], Yen-Hwei Chang [a]

[a] Department of Materials Science and Engineering, National Cheng Kung University, Tainan 701, Taiwan

[b] Department of Safety Health and Environment, Chung Hwa University of Medical Technology, 89 Wen-Hua 1st St., Jen-Te Hsiang, Tainan County, Taiwan

[c] Department of Electronic Engineering, National Formosa University, Huwei, Yunlin 632, Taiwan

Received 9 May 2011; received in revised form 27 September 2011; accepted 3 October 2011

Available online 8 October 2011

Abstract

$Ba_{1-y}Sr_yLa_{4-x}Dy_x(WO_4)_7$ ($x = 0.04–0.2$, $y = 0–0.4$) phosphors were prepared via a solid-state reaction, and their photoluminescence properties were investigated. Under near-UV (388 nm) excitation, the emission spectra of $BaLa_{4-x}Dy_x(WO_4)_7$ exhibited emission peaks in the visible region at 453, 479, and 573 nm, which are assigned to the intra-4*f*-shell transitions from the ($^4M_{21/2} + {}^4I_{13/2} + {}^4K_{17/2} + {}^4F_{7/2} \rightarrow {}^6H_{13/2}$), ($^4F_{9/2} \rightarrow {}^6H_{15/2}$), and ($^4F_{9/2} \rightarrow {}^6H_{13/2}$) transitions, respectively. The concentration quenching effect occurs when the Dy^{3+} concentration is $x = 0.12$ (3 at.%). A partial substitution of Ba^{2+} by Sr^{2+} in $Ba_{1-y}Sr_yLa_{3.88}Dy_{0.12}(WO_4)_7$ can not only enhance the emission intensity of the emission spectra, but also change the phonon relaxation rate and the site symmetry around the Dy^{3+} ions. The optimal condition is at $y = 0.3$ ($Ba_{0.7}Sr_{0.3}La_{3.88}Dy_{0.12}(WO_4)_7$), with CIE coordinates of (0.332, 0.367), corresponding to a near-white color.

Keywords: $BaLa_4(WO_4)_7$; Luminescence; Phosphor; Dysprosium doping

1. Introduction

Oxide phosphors are widely used in solid-state lighting (SSL) technology, such as white-light-emitting diodes (WLEDs), due to their higher chemical stability and resistance to moisture compared to those of sulfide phosphors [1,2]. Currently, the most common WLEDs use an InGaN blue LED chip to excite a yellow-emitting yttrium-aluminum garnet phosphor ($YAG:Ce^{3+}$) proper mixing of the excitation and emission lights produces white light [3,4]. However, this type of white light is not applicable for certain architectural lighting purposes due to its low color rendering index (CRI) and chromatic aberration after a long working period [5]. More recently, single-phase white-light-emitting phosphors have received a lot of attention for application in WLEDs under ultraviolet excitation, which is a possible method to enhance the chromatic stability after a long working period. The single-phase white-light-emitting phosphors can be obtained by mixing two-band emissions in the visible range. Dy^{3+}-doped phosphors have two dominant emission bands of blue and yellow. By adjusting the yellow-to-blue intensity ratio to a suitable value, it is possible to obtain a phosphor with near-white light [6].

For rare-earth ions with a partially filled 4*f* shell, the 4*f* electrons are well shielded by $5s^2$ and $5p^6$ orbitals. Therefore, emission transitions yield sharp lines in optical spectra [7]. Line-type f–f transitions of rare-earth-element-based phosphors can narrow the emissions to the visible range, resulting in high efficiency and high lumen equivalence. Trivalent dysprosium has a $4f^9$ configuration and two dominant emission bands that arise from the $^4F_{9/2} \rightarrow {}^6H_{15/2}$ (blue) and $^4F_{9/2} \rightarrow {}^6H_{13/2}$ (yellow) transitions. Unlike the blue $^4F_{9/2} \rightarrow {}^6H_{15/2}$ transition, the yellow $^4F_{9/2} \rightarrow {}^6H_{13/2}$ emission transition belongs to a hypersensitive transition and is strongly influenced by the chemical environment surrounding Dy^{3+} ($\Delta J = 2$) [7–9]. When doped into a suitable host lattice, Dy^{3+} shows a strong white light emission with excitation bands located in the near-UV to blue region. Hence, there has been growing interest in developing Dy^{3+}-doped phosphors with high absorption in the near-UV to blue range.

Rare-earth tungstates have long attracted attention due to their excellent luminescence properties [10,11]. A number of Eu^{3+}- and Tb^{3+}-activated tungsten oxides have already been

* Corresponding author. Tel.: +886 6 2757575x62928; fax: +886 6 2344393.
E-mail address: wshwang@mail.ncku.edu.tw (W.-S. Hwang).

0272-8842/$36.00
doi:10.1016/j.ceramint.2011.10.006

reported as phosphors [5,10–12]. However, no spectroscopic characterizations of $BaLa_4(WO_4)_7$:Dy^{3+} phosphors have been reported. The basic structure of the monoclinic $BaLa_4(WO_4)_7$ compound was confirmed by Evdokimov and Trunov [13], and the compound was reported as a Eu^{3+}-activated phosphor [14]. In the present work, the luminescence properties of $BaLa_{4-x}Dy_x(WO_4)_7$ are investigated. In order to improve the optical properties of $BaLa_{4-x}Dy_x(WO_4)_7$ phosphors, the effects of substituting Ba^{2+} with Sr^{2+} are also studied.

2. Experimental procedure

Phosphors with compositions of $Ba_{1-y}Sr_yLa_{4-x}Dy_x(WO_4)_7$ were synthesized via a standard solid-state reaction. The starting materials were $BaCO_3$ (Alfa Aesar), $SrCO_3$ (Alfa Aesar), La_2O_3 (SHOWA), WO_3 (Alfa Aesar), and Dy_2O_3 (Alfa Aesar) with purities of 99.99%. The raw materials were weighed according to the stoichiometric ratio and ground by a mechanically activated high-energy vibro-mill for 15 min with zirconia balls in a polyethylene jar. The vibrating mill method is used to modify the properties of materials, to enhance the reactivity of materials, to produce advanced materials, and to separate composite materials into their constituents. When materials are subjected to intensive grinding, their structural and microstructural characteristics greatly change. These structural changes determine the reactivity of materials and play an important role in subsequent processes. The vibrating ball milling method can reduce reagent consumption, decrease the decomposition temperature, and promote the recovery of valuable components of materials [15]. After grinding, the mixtures were calcined at 900 °C for 12 h in air with a heating rate 5 °C/min and they were furnace cooled. The X-ray diffraction (XRD) of the samples was examined on a Rigaku Dmax diffractometer using Cu Kα radiation (λ = 0.15406 nm) with a source power of 30 kV and a current of 20 mA to identify the phases of the product. The excitation and emission spectra of the phosphors were measured with a Hitachi F-4500 fluorescence spectrophotometer using a Xe lamp as the excitation source at room temperature. The Commission Internationale de l'Éclairage (CIE) chromaticity coordinates of the phosphors were calculated from their emission spectra [16] under an excitation wavelength of 388 nm. All measurements were carried out at room temperature.

3. Results and discussion

Fig. 1 shows the powder XRD patterns of $Ba_{1-y}Sr_yLa_{3.88}Dy_{0.12}(WO_4)_7$ (y = 0–0.4) samples. All diffraction peaks are in agreement with JCPDS card no. 29-0177 and no obvious impurity phases appear, indicating that all the samples are single-phase and isostructural to $BaLa_4(WO_4)_7$. Fig. 2(a) shows the lattice parameters for the substitution of La^{3+} by Dy^{3+} ions in $BaLa_{4-x}Dy_x(WO_4)_7$ (x = 0–0.12). The difference in the ionic radius between La^{3+} ions (r = 1.16 Å) and Dy^{3+} ions (r = 0.97 Å) resulted in a decrease of the lattice parameters. The lattice parameters of $Ba_{1-y}Sr_yLa_{3.88}Dy_{0.12}(WO_4)_7$ (y = 0–0.4) estimated from XRD data were shown in Fig. 2(b). The

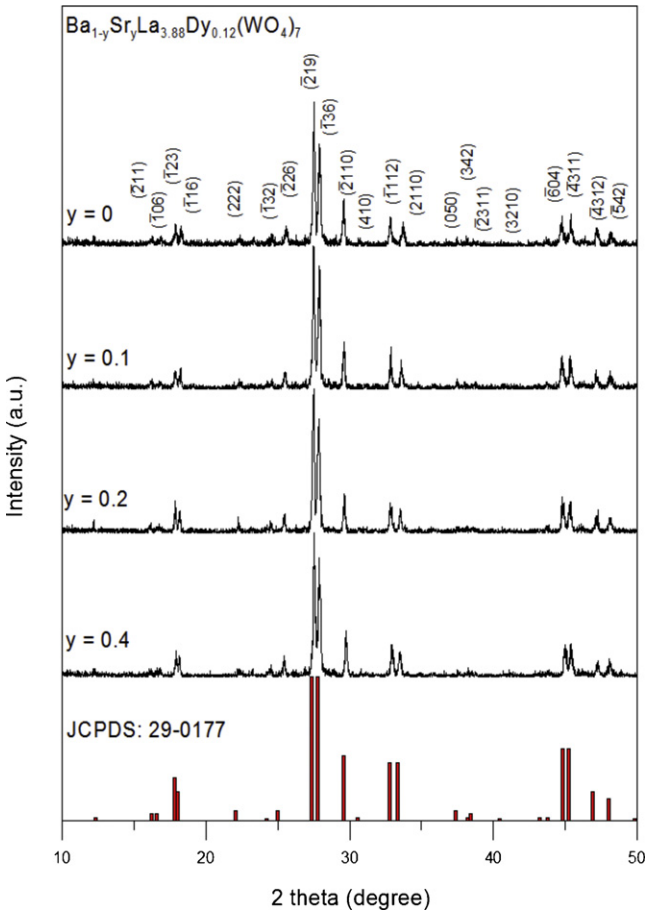

Fig. 1. X-ray diffraction patterns of $Ba_{1-y}Sr_yLa_{3.88}Dy_{0.12}(WO_4)_7$ (y = 0–0.4).

crystal structure gradually shrank along the a, b and c axes with increasing Sr^{2+} content. A linear relationship between the lattice parameters and the concentrations of Sr^{2+} ions was found. This is caused by the difference in ionic radius between Ba^{2+} (r = 1.52 Å) and Sr^{2+} (r = 1.36 Å). These results confirm that Sr^{2+} and Dy^{3+} ions were incorporated into the $BaLa_4(WO_4)_7$ lattice by replacing Ba^{2+} and La^{3+} ions, respectively. $BaLa_{4-x}Dy_x(WO_4)_7$ (x = 0–0.12) and $Ba_{1-y}Sr_yLa_{3.88}Dy_{0.12}(WO_4)_7$ (y = 0–0.4) were considered to be solid solutions because the variations in lattice constants satisfied Vegard's rule [17].

The excitation and emission spectra of $BaLa_{4-x}Dy_x(WO_4)_7$ are shown in Fig. 3. The weak broad peak at 270 nm in the excitation spectra is due to the charge-transfer state (CTS) from O^{2-} to Dy^{3+} [18]. The sharp excitation peaks from 300 to 420 nm can be attributed to the intra-4f forbidden transitions from the ground level $^6H_{15/2}$ to higher energy levels of Dy^{3+} ions [19,20]. The most dominant excitation peak at 388 nm is assigned to the ($^6H_{15/2} \rightarrow {}^4M_{21/2} + {}^4I_{13/2} + {}^4K_{17/2} + {}^4F_{7/2}$) transition. The available strong excitation channels in the near-UV region are suitable for UV-LED conversion. The emission spectra consist of three emission peaks in the visible region, at 453, 479, and 573 nm, respectively, which are assigned to the intra-4f-shell transitions of Dy^{3+} from the ($^4M_{21/2} + {}^4I_{13/2} + {}^4K_{17/2} + {}^4F_{7/2} \rightarrow {}^6H_{13/2}$), ($^4F_{9/2} \rightarrow {}^6H_{15/2}$), and ($^4F_{9/2} \rightarrow {}^6H_{13/2}$) transitions, respectively

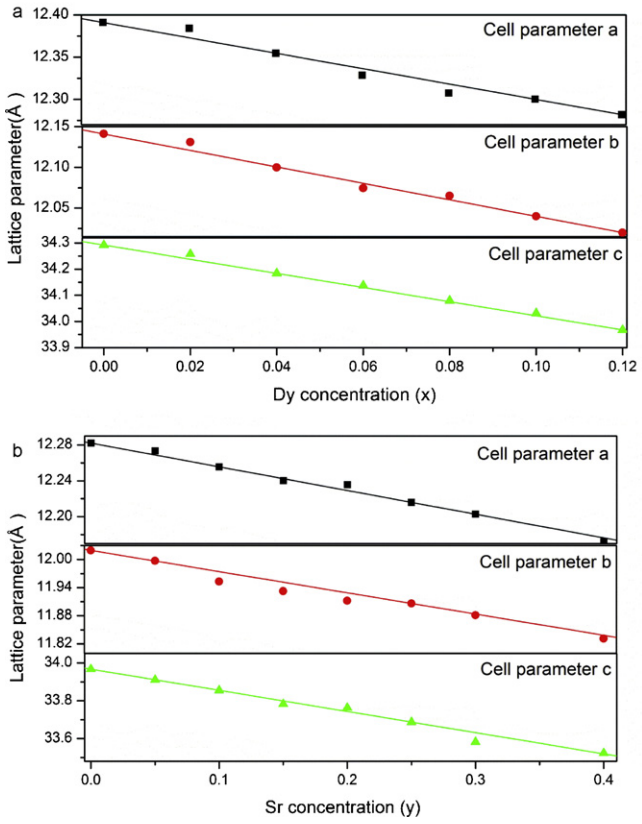

Fig. 2. The variations of the monoclinic lattice parameters (*a*, *b*, and *c* axis) with (a) the Dy^{3+} content in $BaLa_{4-x}Dy_x(WO_4)_7$ ($x = 0$–0.12) (in Å) and, (b) Sr^{2+} content in $Ba_{1-y}Sr_yLa_{3.88}Dy_{0.12}(WO_4)_7$ ($y = 0$–0.4) (in Å).

[21]. The Dy^{3+} concentration changes only the intensity of the emission spectra. The maximum emission intensity was obtained at $x = 0.12$. The $^4F_{9/2} \rightarrow {}^6H_{13/2}$ hypersensitive transition is a force electric dipole transition with $\Delta J = 2$, which is susceptible to the crystal field and occurs only for a low-symmetry lattice with no inversion center. However, the magnetic-dipole-dominated transition $^4F_{9/2} \rightarrow {}^6H_{15/2}$ is invariant to the environment and hardly varies with the crystal field strength because it is

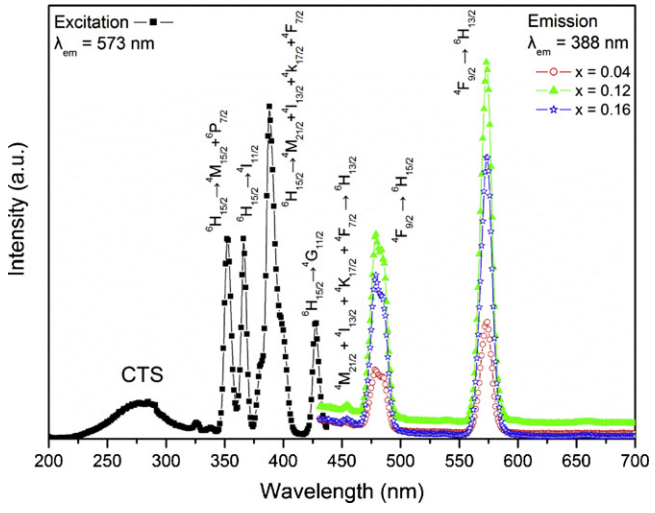

Fig. 3. Excitation and emission spectra of $BaLa_{4-x}Dy_x(WO_4)_7$ ($x = 0.04$–0.2).

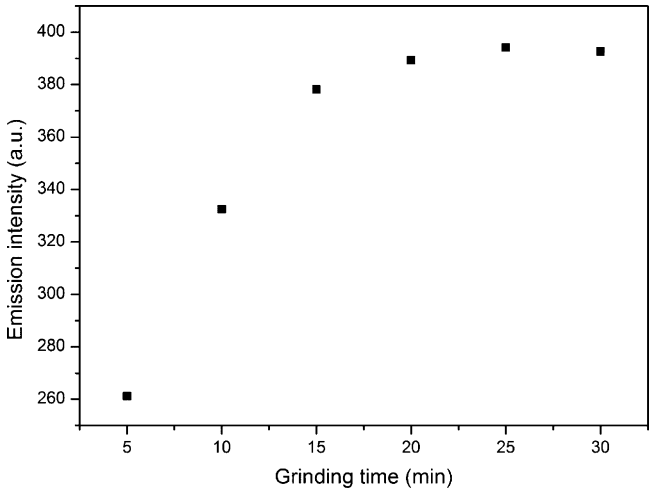

Fig. 4. The relationship of grinding time and emission intensity of the $^4F_{9/2} \rightarrow {}^6H_{13/2}$ transition of $BaLa_{3.88}Dy_{0.12}(WO_4)_7$ under excitation at 388 nm.

parity-allowed [22–24]. Therefore, the emission intensity ratio of the $^4F_{9/2} \rightarrow {}^6H_{13/2}$ and $^4F_{9/2} \rightarrow {}^6H_{15/2}$ transitions, called asymmetry ratio, which can be used as a measure of the site symmetry around the Dy^{3+} ions. In $BaLa_{4-x}Dy_x(WO_4)_7$ phosphors, the emission from the $^4F_{9/2} \rightarrow {}^6H_{13/2}$ transition is more intensive than that from the $^4F_{9/2} \rightarrow {}^6H_{15/2}$ transition, revealing that Dy^{3+} ions occupied low-symmetry local sites with no inversion center.

Fig. 4 shows the relationship of grinding time and emission intensity of the $^4F_{9/2} \rightarrow {}^6H_{13/2}$ transition of $BaLa_{3.88}Dy_{0.12}(WO_4)_7$ under excitation at 388 nm. The vibrating ball milling method can produce unique and metastable materials via a self-sustaining reaction of highly exothermic powder mixtures. The method comprises four processes: (1) material destruction; (2) formation of a new surface; (3) fine grinding; and (4) transformation into a new material with a completely different structure [15]. As shown in Fig. 4, the emission intensity increased rapidly with increasing grinding time until it reached to 20 min. When the grinding time was more than 20 min, the emission intensity increased slightly as grinding time increased. The results show that increasing grinding time can enhance the emission intensity.

The decay curves of the $^4F_{9/2} \rightarrow {}^6H_{13/2}$ transition for various Dy^{3+} concentrations in $BaLa_{4-x}Dy_x(WO_4)_7$ under an excitation wavelength of 388 nm are shown in Fig. 5. The decrease in the emission intensity for Dy^{3+} concentrations greater than $x = 0.12$ is due to the concentration quenching effect in rare-earth-element-doped systems caused by Dy^{3+}–Dy^{3+} mutual interactions [25]. As shown in Fig. 5, the decay curves diverge from a single-exponential decay when the Dy^{3+} concentration is increased to more than $x = 0.12$, indicating that more than one relaxation process exists. The single-exponential decay can be expressed as $I = I_0 \exp(-t/\tau)$, where I_0 and I are the luminescence intensities at time 0 and t, respectively, and τ is the radiative decay time [26]. The radiative decay time τ includes contributions from the energy transfer rate P_{tr}, multiphonon relaxation rate A_{ph}, and radiative lifetime τ_0; i.e., $1/\tau = A_{ph} + P_{tr} + 1/\tau_0$. The single-exponential decay is due to

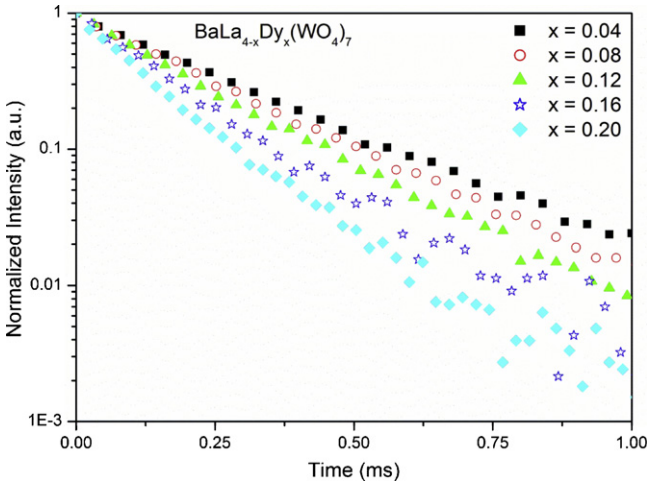

Fig. 5. Normalized decay curves of the $^4F_{9/2} \rightarrow {}^6H_{13/2}$ transition for various Dy^{3+} concentrations in $BaLa_{4-x}Dy_x(WO_4)_7$ under excitation at 388 nm.

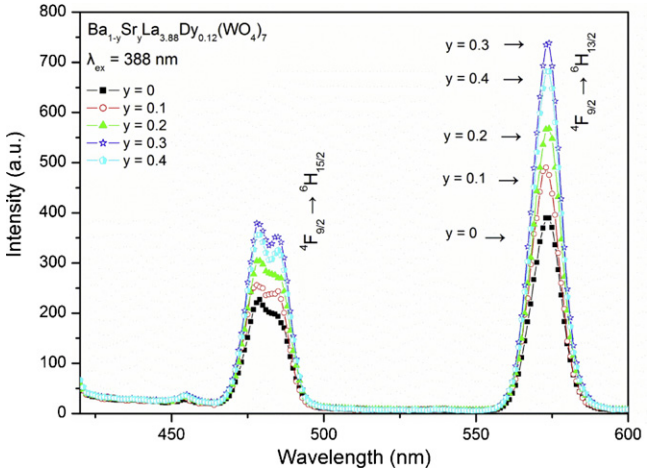

Fig. 7. Emission spectra of $Ba_{1-y}Sr_yLa_{3.88}Dy_{0.12}(WO_4)_7$ (y = 0–0.4) excited at 388 nm.

Dy^{3+} ions occupying only one type of crystallographic site and the radiative time and phonon relaxation rate being identical for all Dy^{3+} ions [6]. However, at higher Dy^{3+} concentrations, the activated centers have different local environments and the associated ions relax at different rates, leading to resonant or phonon-assisted cross-relaxations via matched energy levels between two adjacent active centers. The cross-relaxation scheme has been identified for Dy^{3+} as: $^4F_{9/2}$ (Dy^{3+}I) + $^6H_{15/2}$ (Dy^{3+}II) → $^6H_{9/2}$ (Dy^{3+}I) + $^6F_{1/2}$ (Dy^{3+}II) [27,28], which is shown in Fig. 6.

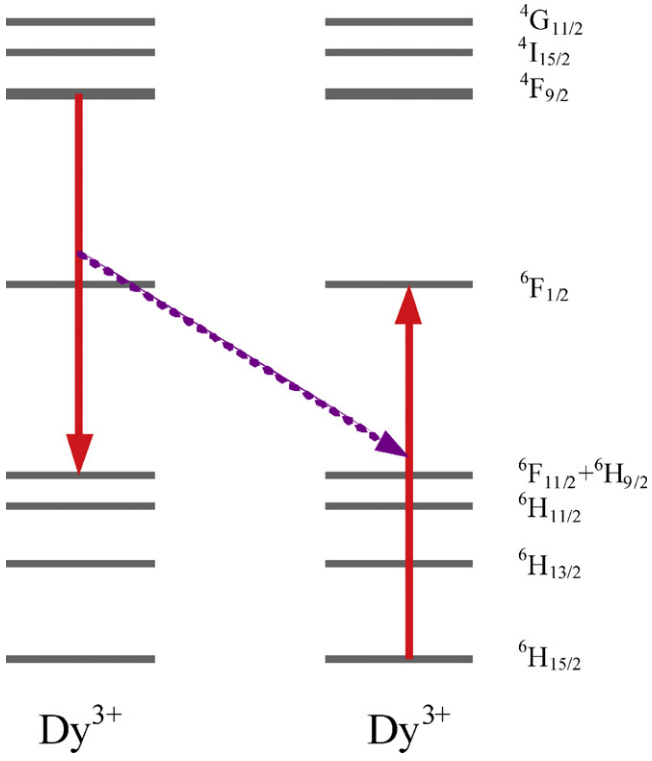

Fig. 6. Schematic diagram of cross-relaxation process between Dy^{3+} ions in $BaLa_2WO_7$. The arrow indicates the amount of energy which is transferred from one ion to the other.

In order to further enhance the luminescence properties of $BaLa_{4-x}Dy_x(WO_4)_7$, Sr^{2+} was introduced to substitute Ba^{2+} in $BaLa_{4-x}Dy_x(WO_4)_7$ to change the crystal field. The optimal condition of $BaLa_{4-x}Dy_x(WO_4)_7$ is $x = 0.12$ ($BaLa_{3.88}Dy_{0.12}(WO_4)_7$). Sr^{2+} was used to partially substitute Ba^{2+} in $BaLa_{3.88}Dy_{0.12}(WO_4)_7$, producing compounds $Ba_{1-y}Sr_yLa_{3.88}Dy_{0.12}(WO_4)_7$.

The emission spectra of $Ba_{1-y}Sr_yLa_{3.88}Dy_{0.12}(WO_4)_7$ (y = 0–0.4) phosphors under excitation at 388 nm are shown in Fig. 7. Increasing Sr^{2+} concentration did not only change the emission intensity of the emission spectra, but also change the ($^4F_{9/2} \rightarrow {}^6H_{13/2}$)/($^4F_{9/2} \rightarrow {}^6H_{15/2}$) asymmetry ratio. The emission intensity of the $^4F_{9/2} \rightarrow {}^6H_{13/2}$ and $^4F_{9/2} \rightarrow {}^6H_{15/2}$ transitions both increased with increasing Sr^{2+} concentration, with a maximum at $y = 0.3$. $Ba_{0.7}Sr_{0.3}La_{3.88}Dy_{0.12}(WO_4)_7$ with a ($^4F_{9/2} \rightarrow {}^6H_{13/2}$)/($^4F_{9/2} \rightarrow {}^6H_{15/2}$) asymmetry ratio = 1.93, and cell parameters $a = 12.19$ (Å), $b = 11.87$ (Å), and $c = 33.58$ (Å). The Sr^{2+} is about 10.5% smaller than Ba^{2+}, therefore, a reduction in the lattice constant was reasonable.

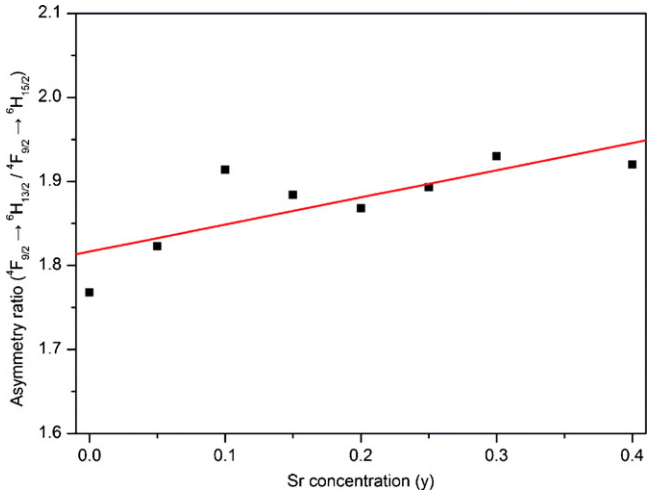

Fig. 8. The dependence of asymmetry ratio on Sr^{2+} concentration in $Ba_{1-y}Sr_yLa_{3.88}Dy_{0.12}(WO_4)_7$ under excitation at 388 nm.

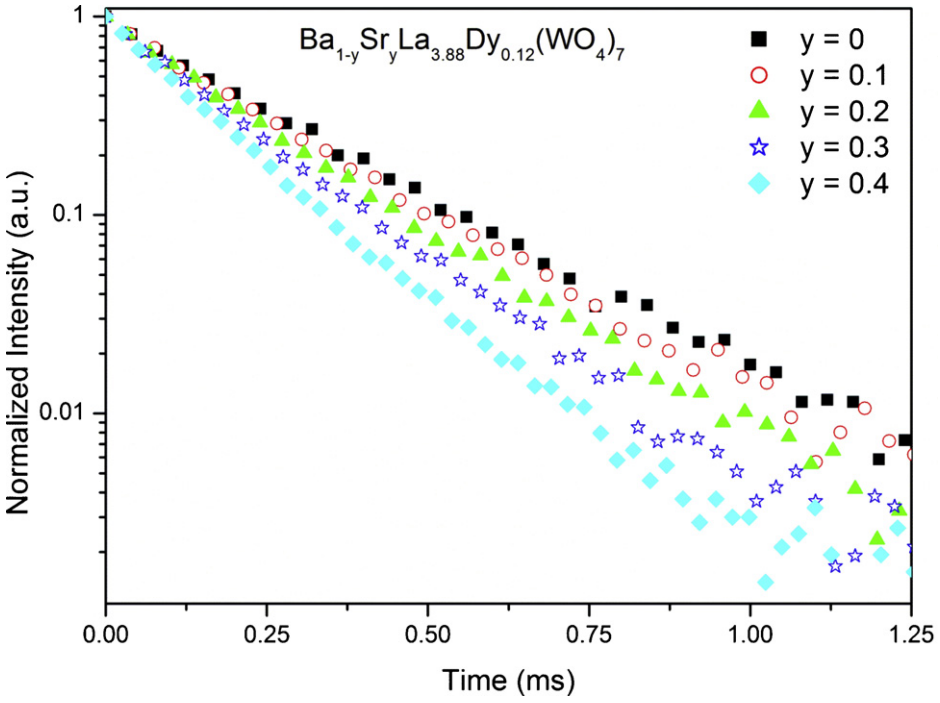

Fig. 9. Normalized decay curves of the $^4F_{9/2} \rightarrow {}^6H_{13/2}$ transition for various Sr^{2+} concentrations in $Ba_{1-y}Sr_yLa_{3.88}Dy_{0.12}(WO_4)_7$ ($y = 0$–0.4) under excitation at 388 nm.

The reduction in the *a*-axis was calculated to be about 0.64% from $y = 0$ to $y = 0.3$, while the reduction in the *b* and *c*-axis were 1.21% and 1.15%, respectively. The reduction in the *a*-axis was much smaller than *b* and *c*-axis. Some induced odd-parity distortions might be expected for $Ba_{1-y}Sr_yLa_{3.88}Dy_{0.12}(WO_4)_7$ in the Sr-substituted compounds. As a consequence, the luminescence properties and the local site symmetry around the Dy^{3+} ions might be changed, and an increased asymmetry ratio was expected. Fig. 8 shows the ($^4F_{9/2} \rightarrow {}^6H_{13/2}$)/($^4F_{9/2} \rightarrow {}^6H_{15/2}$) asymmetry ratio on Sr^{2+} concentration in $Ba_{1-y}Sr_yLa_{3.88}Dy_{0.12}(WO_4)_7$ ($y = 0$–0.4) phosphors under an excitation wavelength of 388 nm. The asymmetry ratio increased from 1.77 to 1.92 as the Sr^{2+} concentration increased from $y = 0$ to $y = 0.4$, revealing that the local structural symmetry around Dy^{3+} ions significantly changed as Sr^{2+} became incorporated into $Ba_{1-y}Sr_yLa_{3.88}Dy_{0.12}(WO_4)_7$. The results indicate that the substitution of Ba^{2+} by Sr^{2+} in $Ba_{1-y}Sr_yLa_{3.88}Dy_{0.12}(WO_4)_7$ can further enhance the emission intensity and decrease the local environment symmetry around Dy^{3+} ions. Since the relative intensities of the $^4F_{9/2} \rightarrow {}^6H_{13/2}$ and the $^4F_{9/2} \rightarrow {}^6H_{15/2}$ emission transitions can be tuned by the Sr^{2+} content, the Commission Internationale de l'Éclairage (CIE) chromaticity coordinates of $Ba_{1-y}Sr_yLa_{3.88}Dy_{0.12}(WO_4)_7$ phosphors varied from (0.332, 0.367) at $y = 0$ to (0.338, 0.372) at $y = 0.4$, corresponding to a near-white color. At the same time, the quantum yield of $BaLa_{3.88}Dy_{0.12}(WO_4)_7$ ($y = 0$) and $Ba_{0.7}Sr_{0.3}La_{3.88}Dy_{0.12}(WO_4)_7$ ($y = 0.3$) were calculated to be 0.47 and 0.51, respectively, under the UV excitation at 388 nm.

Fig. 9 shows the decay curves of the $^4F_{9/2} \rightarrow {}^6H_{13/2}$ transition for various Sr^{2+} concentrations in $Ba_{1-y}Sr_yLa_{3.88}Dy_{0.12}(WO_4)_7$ under an excitation wavelength of 388 nm. The decay rate varied with different Sr^{2+} concentrations, indicating that the incorporation of Sr^{2+} into $Ba_{1-y}Sr_yLa_{3.88}Dy_{0.12}(WO_4)_7$ provided extra decay channels. The local environment and phonon relaxation rate are different for Dy^{3+} ions at different Sr^{2+} concentrations, which provided an evidence that the site symmetry changed with increasing Sr^{2+} concentration.

4. Conclusion

Near-white-emitting phosphors $Ba_{1-y}Sr_yLa_{4-x}Dy_x(WO_4)_7$ were synthesized via a standard solid-state reaction. The excitation spectra show strong excitation peaks in the near-UV region, making the phosphors candidates for UV-LED conversion. The emission intensity of the $^4F_{9/2} \rightarrow {}^6H_{13/2}$ transition is higher than that of the $^4F_{9/2} \rightarrow {}^6H_{15/2}$ transition, revealing that Dy^{3+} ions occupied low-symmetry local sites with no inversion center in $BaLa_4(WO_4)_7$. The concentration quenching effect occurs when the Dy^{3+} concentration is $x = 0.12$ (3 at.%), indicating that Dy^{3+} ions occupied single crystallographic sites for Dy^{3+} concentrations below 3 at.%. A partial substitution of Ba^{2+} by Sr^{2+} in $Ba_{1-y}Sr_yLa_{3.88}Dy_{0.12}(WO_4)_7$ can not only enhance the emission intensity of the emission spectra, but also change the phonon relaxation rate and the site symmetry around the Dy^{3+} ions. The substitution of Ba^{2+} by Sr^{2+} distorts the crystal. The optimal condition is at $y = 0.3$ ($Ba_{0.7}Sr_{0.3}La_{3.88}Dy_{0.12}(WO_4)_7$) with cell parameters $a = 12.19$ (Å), $b = 11.87$ (Å), and $c = 33.58$ (Å). The reduction in the *a*-axis (0.64%) was much smaller than *b* (1.21%) and *c*-axis (1.15%). The increase in the asymmetry ratio provided a convincing evidence for the site symmetry degradation around the Dy^{3+} ions in the Sr-substituted samples. Consequently, the color of Sr-substituted phosphors, $Ba_{1-y}Sr_yLa_{3.88}Dy_{0.12}(WO_4)_7$

can be tuned by increasing Sr^{2+} content. $Ba_{0.7}Sr_{0.3}La_{3.88}Dy_{0.12}(WO_4)_7$ with CIE coordinates at (0.332, 0.367), corresponding to a near-white color.

Acknowledgement

The authors would like to thank the Bureau of Energy, Ministry of Economic Affairs in Taiwan, for financially supporting this research under grant 100-D0204-2.

References

[1] P. Li, Z. Wang, Z. Yang, Q. Guo, X. Li, Emission features of $LiBaBO_3:Sm^{3+}$ red phosphor for white LED, Mater. Lett. 63 (2009) 751–753.
[2] V. Sivakumar, U.V. Varadaraju, Intense red-emitting phosphors for white light emitting diodes, J. Electrochem. Soc. 152 (2005) H168.
[3] K. Zhang, W. Hu, Y. Wu, H. Liu, Influence of processing techniques on the properties of YAG:Ce nanophosphor, Ceram. Int. 35 (2009) 719–723.
[4] S.H. Lee, H.Y. Koo, S.M. Lee, Y.C. Kang, Characteristics of $Y_3Al_5O_{12}$:Ce phosphor powders prepared by spray pyrolysis from ethylenediaminetetraacetic acid solution, Ceram. Int. 36 (2010) 611–615.
[5] K.S. Hwang, S. Hwangbo, J.T. Kim, Sol–gel synthesis of red-emitting $LiEuW_2O_8$ powder as a near-ultraviolet convertible phosphor, Ceram. Int. 35 (2009) 2517–2519.
[6] C.H. Liang, X. Qi, Y.S. Chang, Color tone tuning by partial Sr^{2+} substitution of Ba^{2+} in the white phosphors $Ba_{1-y}Sr_yLa_{2-x}Dy_xZnO_5$ ($x = 0.01$–0.2, $y = 0$–0.65), J. Electrochem. Soc. 157 (5) (2010) J169–J174.
[7] G. Bhaskar Kumar, S. Buddhudu, Synthesis and emission analysis of RE^{3+} (Eu^{3+} or Dy^{3+}):Li_2TiO_3 ceramics, Ceram. Int. 35 (2009) 521–525.
[8] Q. Su, J. Lin, B. Li, A study on the luminescence properties of Eu^{3+} and Dy^{3+} in $M_2RE_8(SiO_4)_6O_2$ (M = Mg, Ca; RE = Y, Gd, La), J. Alloys Compd. 225 (1995) 120–123.
[9] G. Jia, Y. Song, M. Yang, Y. Huang, L. Zhang, H. You, Uniform $YVO_4:Ln^{3+}$ (Ln = Eu, Dy, and Sm) nanocrystals: solvothermal synthesis and luminescence properties, Opt. Mater. 31 (2009) 1032–1037.
[10] C.H. Chiu, C.H. Liu, S.B. Huang, T.M. Chen, Synthesis and luminescence properties of intensely red-emitting $M_5Eu(WO_4)_{4-x}(MoO_4)_x$ (M = Li, Na, K) phosphors, J. Electrochem. Soc. 155 (3) (2008) J71–J78.
[11] L.G. Jacobsohn, K.B. Sprinkle, C.J. Kucera, T.L. James, S.A. Roberts, H. Qian, E.G. Yukihara, T.A. Devol, J. Ballato, Synthesis, luminescence and scintillation of rare earth doped lanthanum fluoride nanoparticles, Opt. Mater. 33 (2010) 136–140.
[12] C.H. Chiu, C.H. Liu, S.B. Huang, T.M. Chen, White-light-emitting diodes using red-emitting $LiEu(WO_4)_{2-x}(MoO_4)_x$ phosphors, J. Electrochem. Soc. 154 (7) (2007) J181–J184.
[13] A.A. Evdokimov, V.K. Trunov, Investigation of certain tungstate systems, Russ. J. Inorg. Chem. 18 (10) (1973) 1506.
[14] G. Blasse, G.J. Dirksen, L.H. Brixner, The luminescence of Eu^{3+}-activated $BaLa_4(WO_4)_7$, Mater. Chem. Phys. 21 (1989) 293.
[15] K. Tkacova, Mechanical Activation of Minerals, Elsevier, Amsterdam, 1989.
[16] R.W.G. Hunt, The Reproduction of Color in Photography, Printing & Television, Fountain Press, London, 1987.
[17] B.D. Cullity, S.R. Stock, Elements of X-ray Diffraction, Prentice-Hall, Englewood Cliffs, NJ, 2001, p. 339.
[18] H. Lai, A. Bao, Y. Yang, W. Xu, Y. Tao, H. Yang, Preparation and luminescence property of Dy^{3+}-doped YPO_4 phosphors, J. Lumin. 128 (2008) 521.
[19] I. Omkaram, S. Buddhudu, Photoluminescence properties of $MgAl_2O_4:Dy^{3+}$ powder phosphor, Opt. Mater. 32 (2009) 8–11.
[20] P.L. Dai, B.S. Tsai, Y.Y. Tsai, H.L. Chen, T.H. Feng, K.H. Liao, Y.S. Chang, Synthesis and luminescence properties of $YInGe_2O_7$ phosphors activated by dysprosium ions, Opt. Mater. 32 (2009) 392–397.
[21] C.Y. Li, Y.H. Chang, Y.F. Lin, Y.S. Chang, Y.J. Lin, Synthesis and luminescent properties of Ln^{3+} (Eu^{3+}, Sm^{3+}, Dy^{3+})-doped lanthanum aluminum germinate $LaAlGe_2O_7$ phosphors, J. Alloys Compd. 439 (2007) 367–375.
[22] B.R. Judd, Optical absorption intensities of rare-earth ions, Phys. Rev. 127 (1962) 750.
[23] G.S. Ofelt, Intensities of crystal spectra of rare-earth ions, J. Chem. Phys. 37 (1962) 511.
[24] S. Shionoya, W.M. Yen, Phosphor Handbook, CRC, Boca Raton, FL, 1999 (Chap. 5, p. 179).
[25] X.Q. Su, B. Yan, The synthesis and luminescence of $YP_xV_{1-x}O4:Dy^{3+}$ microcrystalline phosphors by in situ co-precipitation composition of hybrid precursors, Mater. Chem. Phys. 93 (2005) 552.
[26] N. Shanta Singh, R.S. Ningthoujm, N. Yaiphaba, S. Dorendrajit Singh, R.K. Vasta, Lifetime and quantum yield studies of Dy^{3+} doped $GdVO_4$ nanoparticles: concentration and annealing effect, J. Appl. Phys. 105 (2009) 064303.
[27] L. Nagli, D. Bunimovih, A. Katzir, O. Gorodetsky, V. Molev, The luminescence properties of Dy-doped $SrSiO_3$, J. Non-Cryst. Solids 217 (1997) 208–214.
[28] Y. Dwivedi, S.B. Rai, Spectroscopic study of Dy^{3+} and Dy^{3+}/Yb^{3+} ions co-doped in barium fluoroborate glass, Opt. Mater. 31 (2009) 1472–1477.